Characterisation of heat-treated Ti-rich NiTi fabricated by laser powder bed fusion

Londiwe Motibane[1,2*], *Lerato* Tshabalala[1], *Thorsten* Becker [2,3,4], Hosia Kgomo[1]

[1] Laser Enabled Manufacturing, Photonics Center, Council for Scientific and Industrial Research, Meiring Naudè Road, Brummeria, Pretoria, 0184, South Africa.
[2] Centre for Materials Engineering, University of Cape Town, Library Rd, Cape Town, 7701, South Africa.
[3] Department of Mechanical and Mechatronic Engineering, Stellenbosch University, Joubert street, Stellenbosch 7602, South Africa.
[4] eNtsa, Nelson Mandela University, North campus, Gardham Avenue, Summerstrand, Gqeberha, South Africa.

Abstract. Nitinol (NiTi) is useful for biomedical applications, and laser-powder bed fusion (L-PBF) presents a unique opportunity to fabricate complex and patient-specific implant designs. The processing of nitinol via L-PBF, however presents a challenge as it results in an inhomogeneous microstructure that affects mechanical performance and can limit functional property performance. Moreover, an understanding of Ti-rich NiTi processed via L-PBF is lacking. Post-processing heat treatments are an avenue to alter and tailor the microstructure and thus influence the resulting phase transformations and mechanical performance. This paper presents various heat treatments and the influence of their resultant microstructures, phases and transformation temperature behaviour is characterised.

1 Introduction

Nitinol (NiTi) is a shape memory alloy exhibiting shape memory effect and superelasticity. These functional properties are driven by a solid-state transformation from a low-temperature martensite phase to a high-temperature austenite phase. When deformed, nitinol can recover its original shape after being heated (shape memory effect) or after unloading (superelasticity). Besides its functional properties, it has good biocompatibility, high corrosion resistance, excellent mechanical properties, and abrasion resistance [1]. Such properties lend it well to use in biomedical, aerospace and automotive applications. However, NiTi's phase transformation and superelastic properties are highly sensitive to composition and constituent phases—for instance, an increase in Ni content by 0.5 at. % reduces the austenite finish temperature (Af) of the alloy by about 50 °C [1]. This makes the fabrication of nitinol components challenging.

Laser powder bed fusion (L-PBF) is an attractive fabrication method for customised complex components [1, 2]. Challenges such as Ni evaporation leading to compositional deviations, Ti oxidation and unwanted precipitation formation during printing and post-

processing still exist in processing NiTi via L-PBF [2, 3]. Poor mechanical and superelastic properties due to microstructure inhomogeneity, porosity and residual stresses have been reported to limit the proper functionality of printed NiTi [4, 5]. Thus, the L-PBF of NiTi has proved to be challenging in meeting the required properties for biomedical applications. Post-fabrication heat treatment can modify the microstructure and properties of additively manufactured NiTi by restoring ductility, relieving residual stresses, and, most importantly, allowing for the suitable tailoring of transformation temperatures of NiTi alloys [2-6].

Post-processing heat treatment is an avenue to be explored to modify phase transformation and mechanical properties as it is effective in doing so [3,4,7,8]. Most of these studies are based on the heat treatment of Ni-rich NiTi, and very few treat Ti-rich NiTi alloys. Of the few that focused on Ti-rich NiTi, Lu et al. [8] investigated the influence of multi-stage heat treatment of L-PBF-produced Ti-rich (Ni49.4Ti50.6 at.%) nitinol. The multi-stage heat treatment transformed nanoscale $NiTi_2$ precipitates into homogeneously distributed globular precipitates, which led to a high tensile strain of 22.4 ± 0.4% and a high ultimate tensile strength of 880 ± 13MPa. Monu et al. [4] investigated the heat treatment of NiTi alloys and found that ageing treatments resulted in substantial grain restructuring. Differential scanning calorimeter curves of aged-treated samples exhibited narrow transformation intervals and more pronounced phase transformations than as-built samples [3]. Research on developing heat treatments for suitable functionality of L-PBF NiTi at body temperature is scarce. The aim of the study is to characterise the microstructure, functional and mechanical properties of heat treated Ti-rich NiTi fabricated via L-PBF.

2 Materials and methods

2.1 Material and processing

This study used gas-atomised nitinol powder of composition Ti 52.15at% and Ni 47.8 at%. The powder had a spherical morphology and sizes 65 ±20 µm[9]. Figure 1 below show the SEM micrograph at 100X and 1000X magnification. The powder was processed to fabricate test specimens on a Concept Laser MLab 200R (General Electric, USA) system with these processing parameters: laser power of 95 W scanning speed of 600 mm/s, hatch spacing of 85 µm, and a layer thickness of 25 µm. This was carried out in an argon atmosphere. Ten cylinders of 4 mm diameter and 8 mm height were manufactured for compression testing and ten 8 mm diameter and 16 mm height cylinders were manufactured to be used for microscopy, differential scanning carilometry (DSC) and X-ray diffraction (XRD) analyses. These were built in the XY plane and the cylinder height parallel to the build direction in the Z plane. One set of three (4 x 8 mm) cylinders and three (8 x 16 mm) cylinders was left in the as-built condition and it's functional and mechanical properties were studied and published in Motibane et al. [10].

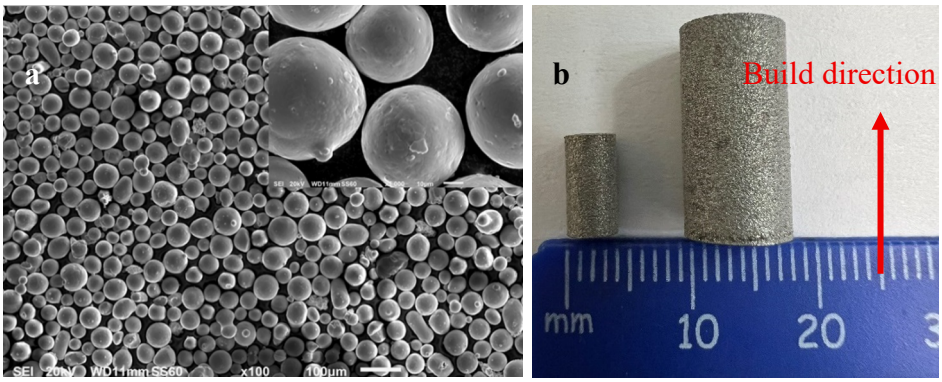

Fig. 1. (a) SEM powder particle analysis at 100X and 1000X. (b) Cylindrical test specimen.

2.2 Heat treatments

The specimens were subjected to heat treatment in an argon-rich Carbolite STF 16/180 tube furnace (Carbolite, UK), and the ramp-up rate was set to 10℃/minute. The first set of specimens was heated to 500 ℃ and held for 30 minutes (HT-500), and the second set was heated to 900 ℃ and held for 4 hours (HT-900). All specimens were water-quenched after the treatment.

2.3 Characterisation

The as-built, HT-500 and HT-900 specimens were sectioned in the transverse direction revealing the XY-plane (perpendicular to building direction). The analysed specimens were prepared by mounting in epoxy resin, grinding with SiC paper, and polishing with diamond and colloidal silica suspensions (Struers Mol 3 µm and OPS 0.25 µm). They were etched to reveal the microstructure using Kroll's reagent. Microscopy was performed on a Jeol JSM-6010 Plus Scanning Electron Microscope (SEM) (Jeol, Japan) and the Tesca MIRA 3 SEM (Tescan Group, Czech Republic) at various magnifications. Phase analysis was achieved using the PANalytical X'pert PRO diffractometer (Malvern Panalytical, South Africa) fitted with a Cu Kα ($\lambda = 0.154$ nm) radiation source. The current was 40 mA, voltage 45 kV and scanning range of 4.995 – 90° 2θ and a step size of 0.02° 2θ. The data was processed using the Xpert Highscore software (Malvern Panalytical, South Africa). Transformation behaviour was determined by differential scanning calorimeter (DSC) on the TA-DSC 8500 calorimeter (TA Instruments, USA). The test temperature range was 0 ℃ to 200 ℃ at heating and cooling rates of 10 ℃/min. As most biomedical implants are under a compression type of stress, compression testing was carried out. Three cylindrical specimens per heat-treated condition underwent compression testing on an Instron servo-hydraulic system with a 50 kN rated load cell at a test rate of 0.5 mm/min (Instron, USA). This was carried out according to the ASTM E9 - 09 standard. Hardness testing was carried out on a Matsuzawa Seiki Vickers MHT−1 micro-hardness machine (Matsuzawa, Japan). A diamond type indenter was used and a force of 0.3 kgf was applied with a dwell time of 10 s. Three hardness run were measured per sample and the average was calculated as the hardness of the material.

3 Results

3.1 Microstructure

Figure 2 shows secondary electron (SE) images of the microstructure of As-built and heat-treated specimens at various magnifications. The micrographs were analysed from the XY-plane (perpendicular to the build direction). The ThAs-built show the laser scans during from processing (Figure 2a). The difference in microstructure is distinct post heat treatment where the AM characteristic scan lines disappear after heat treatment

While the As-built structure, Figure 2a & d showed heterogeneous microstructures in different morphologies, the HT-500 in Figure 2b showed a uniform basket weave structure visible at higher magnification (2000 x) in Figure 2h. The HT-900 in Figure 2c, on the other hand, had a fine cellular microstructure with no distinguishable grain boundaries. The darker phases on the HT-900 are associated with Ti rich phases such as the intermetallic precipitate of $NiTi_2$ evident in Figure 2f & i. This is later discussed in the XRD results.

Closer investigation at higher magnifications of 5000 x, Figure 3a shows three different types of morphologies of the as-built microstructure; the coarse dendritic (A) is the dominating structure resulting from solidification kinetics for alloy systems at a faster cooling rate. Supercooling of the melt pool and the solidification structure yield a basket weave (B), and fine cellular (C) as noted in these areas. The homogenised structure HT-900 shows a fine cellular microstructure at higher magnifications, as shown in Figure 3b.

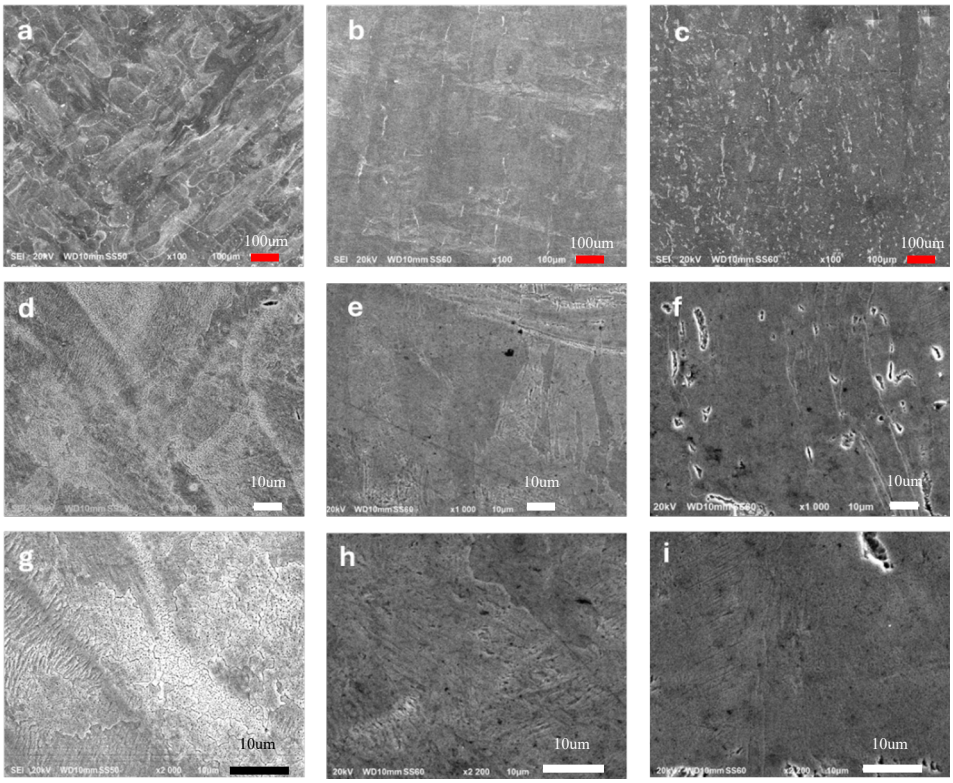

Fig. 2. Micrographs of structure of As-built (a, d, g), HT-500 (b, e, h) and HT-900 (c, f, i), specimen.

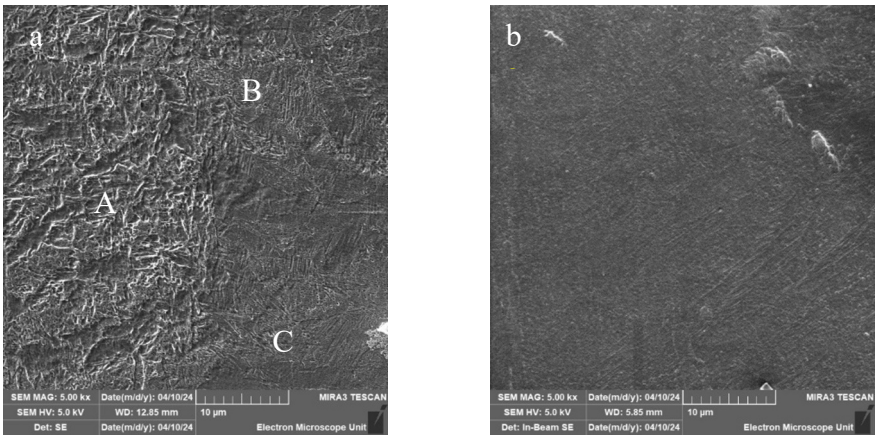

Fig. 3. SEM micrographs of a) As-built and b) HT-900 at higher magnification (5000 x).

3.2 XRD

Figure 4 displays phase analysis on XRD spectra and reveals the different phase peaks and compositions. Distinct austenite and martensite phases characterised the as-built condition. No other phases or precipitates were picked up by XRD, suggesting that no other phases were formed by L-PBF fabrication or that their contents were too little to be picked up by XRD. After heat treatment, the presence of other phases is apparent. The intermetallic precipitate of $NiTi_2$ dominated the HT-500 specimens. The HT-900 exhibited a substantial TiO_2 phase, along with the $NiTi_2$ intermetallic phase.

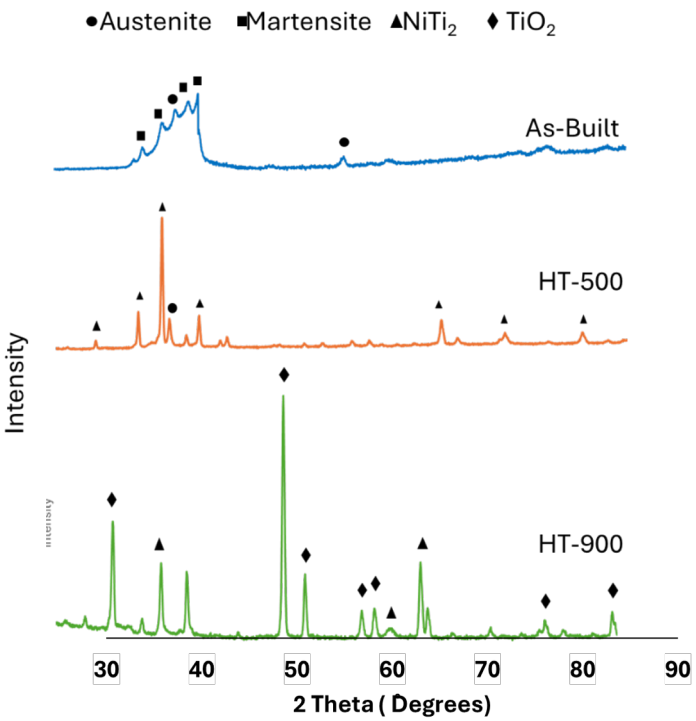

Fig. 4. XRD spectra of As-built, HT-500 and HT-900 NiTi fabricated by L-PBF.

3.3 DSC

The DSC curves for the specimen are given in Figure 5 with the values of Ms, Mf, As, Af, Ms-Mf and As-Af are summarised in Table 1. A single-stage transformation between austenite and martensite is observed in all treatment conditions. A heat treatment at 500 °C transforms martensite into austenite at a lower temperature with lower As and Af temperatures compared to the as-built condition. After treatment at 900 °C, when cooling, martensite formation from austenite occurs at higher temperatures, with an Mf temperature of 40°C. The HT-900 displayed narrower curves, indicating a low transformation range. The lower peak height than the HT-500 specimen signifies that phase transformation was less pronounced.

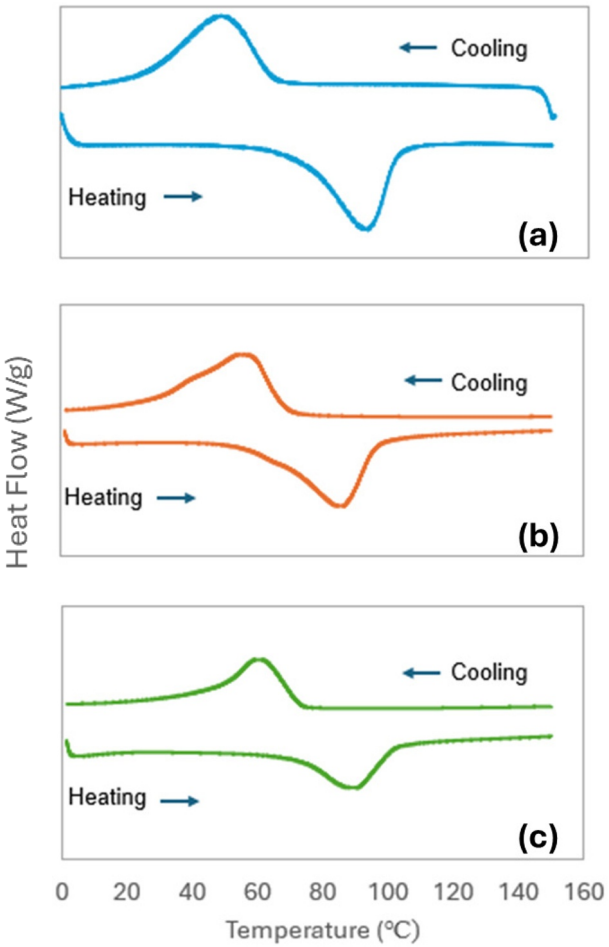

Fig. 5. XRD spectra of NiTi fabricated by L-PBF in the a) As-built, after b) HT-500 and c) HT-900.

Table 1. Transformation values form DSC curves.

	Ms (°C)	Mf (°C)	As (°C)	Af (°C)	Ms -Mf (°C)	As – Af (°C)
As-built [10]	65	22	73	102	43	29
HT-500	68	23	56	97	45	41
HT-900	75	40	70	102	35	35

3.4 Mechanical properties

The compression and hardness results are shown in Figure 6 and Table 2 below. While the As-built condition showed a high Ultimate Compressive Strength (UCS) and lower elongation, heat-treating more than doubled the elongation of HT-500 and HT900 specimens from 11.8 % to 26.3% and 26.5%, respectively. The HT-500 specimen also had a high UCS of 1815 MPa. Heat treatment also increased the hardness, as shown in Figure 6.

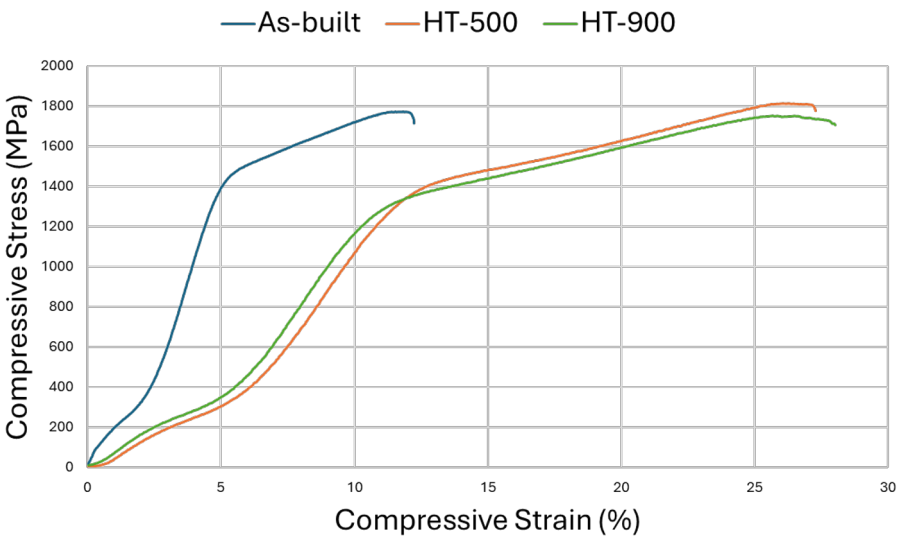

Fig. 6. Compressive stress-strain plot and hardness values of the As-built, HT-500 and HT-900 tested at room temperature.

Table 2. Compressive and hardness values of the As-built, HT-500 and HT-900 specimen.

	UCS (MPa)	Elongation (%)	Hardness (HV)
As-built [10]	1780	11.8	124.8 ± 14
HT-500	1815	26.3	214.5 ± 8
HT-900	1754	26.5	135.8 ± 5

The compressive stress-strain curves also show double yield features in all conditions. The first occurs at 360 MPa and can be associated with the plastic strain by martensite detwinning, while the second yield at 1400 MPa is associated with the onset of dislocation activity [11, 12]. The As-built sample stress plateau at about 2% strain extending to 5% strain, while heat treated samples plateau further at about 6% strain extending to 12% strain. This implies that the martensite dislocation occurs more readily post heat treatment. The As-built however, was strain-hardened earlier than the heat-treated samples.

4 Discussion

The As-built microstructure was inhomogeneous with areas of different morphologies. The effect of heat treatment was evident in the HT-500 and HT-900 structures. There, the microstructure became more homogeneous, with HT-500 exhibiting a basketweave structure and treatment at 900 ℃, resulting in a fine cellular microstructure. The dendritic in the as-built limited elongation to only 11.8%. The higher elongation values of 26.3% and 26.5% can be attributed to homogeneity in HT-500 and HT-900 specimens. Notably, the basket weave microstructure of the HT-500 specimens resulted in slightly increased strength at fracture and higher hardness than the as-built and HT-900 specimens.

For the As-built specimen, XRD indicated the presence of both martensite and retained austenite; the high-temperature austenite phase is retained due to high cooling temperatures in L-PBF [7]. The XRD spectra of the HT-500 specimen showed the presence of the $NiTi_2$ precipitates. These precipitates were not visible in the SEM, possibly due to inadequate observation magnification. Previous studies have shown that the presence of NiT_2 precipitates increases hardness because they restrict dislocation movement [2]. This is also the case in this study, although the elongation was still higher than reported in Tareq et al. [2]. The TiO_2 surface oxide picked up on the HT-900 by XRD is known to be caused by the ageing process [4,8] or oxygen pickup in the furnace.

The HT-900 homogenised the microstructure and composition, which is evident in the narrower transformation ranges, as observed in Tareq et al.[2] and Lu et al.[8]. The increased Mf-Ms and Af-As of the As-built and HT-500 can be attributed to local microstructure inhomogeneity [2,8,11]. Also, this transformation through the R-phase has been attributed to local stresses and composition heterogeneity, such as precipitates and third-element doping [12].

5 Conclusion

Characterisation of heat-treated Ti-rich NiTi fabricated via L-PBF was carried out in this study. The following observations were made:

- Heat treatments significantly affected the microstructure of NiTi. With As-built and HT-500, the inhomogeneous microstructure was transformed into a basketweave microstructure and, with HT-900, into a homogenised fine cellular structure.
- XRD detected $NiTi_2$ precipitates in the HT-500, and TiO_2 was detected together with the $NiTi_2$ in the HT-900.
- Heat treatments increased the elongation compared to the As-built condition. Furthermore, the HT-500 showed increased strength and hardness.
- Microstructural homogeneity also influenced transformation temperature ranges. Where inhomogeneity increased transformation temperatures and a homogeneous structure narrowed to transformation temperature ranges.

References

1. E. Farber, J.N. Zhu, A. Popovich, and V. Popovich, A review of NiTi shape memory alloy as a smart material produced by additive manufacturing. Materials Today: Proceedings, **30,** (2020). https://doi.org/10.1016/j.matpr.2020.01.563
2. S. Tareq, T. Rahman, B. Poudel, H. Chung and P. Kwon. Heat treatment protocol for additively manufactured nitinol shape memory alloys in biomedical applications. Mat. Sci. and Eng. **A**, 897, (2024). https://doi.org/10.1016/j.msea.2024.146274
3. M.B. Abrami, M. Tocci, K. Tamilselvam, D. Brabazon, and A. Pola, Effect of Heat Treatments on Microstructure and Mechanical Properties of Nitinol Prototype Stents Produced by Laser Powder Bed Fusion. Key Eng. Mat., **967**, 143-149, (2023). https://doi.org/10.4028/p-M7D9Cr
4. M.C. Monu, S. Kumar, and D. Brabazon. Heat treatment of NiTi alloys: Influence of volumetric energy density on ageing parameters and the resulting physical properties. J. of Mat. research and tech., **26,** 9532-9555, (2023). https://doi.org/10.1016/j.jmrt.2023.09.251
5. X. Wang, J. Yu, J. Liu, L. Chen, Q. Yang, H. Wei, J. Sun, Z. Wang, Z. Zhang, G. Zhao, J. Van Humbeeck, Effect of process parameters on the phase transformation behavior and tensile properties of NiTi shape memory alloys fabricated by selective laser melting, Addit. Manuf. **36,** 101545, (2020). https://doi.org/10.1016/j.addma.2020.101545
6. P. Jamshidi, C. Panwisawas, E. Langi, S.C. Cox, J. Feng, L. Zhao, M.M. Attallah, Development, characterisation, and modelling of processability of nitinol stents using laser powder bed fusion, J. Alloys Compd. **909,** 164681, (2022). https://doi.org/10.1016/j.jallcom.2022.164681
7. J.J. Marattukalam, V.K. Balla, M. Das, S. Bontha, and S.K. Kalpathy. Effect of heat treatment on microstructure, corrosion, and shape memory characteristics of laser deposited NiTi alloy. J. Alloys Compd, **744**, 337-346, (2018). https://doi.org/10.1016/j.jallcom.2018.01.174
8. H.Z. Lu, L.H. Liu, C. Yang, X. Luo, C.H. Song, Z. Wang, Z., J. Wang, Y.D. Su, Y.F. Ding, I.C. Zhang. and Y.Y. Li. Simultaneous enhancement of mechanical and shape memory properties by heat-treatment homogenization of Ti2Ni precipitates in TiNi shape memory alloy fabricated by selective laser melting. J. Mat. Sci. & Tech., **101**, 205-216, (2022). https://doi.org/10.1016/j.jmst.2021.06.019
9. Y. Yang, Z.G. Wu, B.Y. Shen, M.Z. Wu, Z.S. Yuan, C.Y. Wang, and L.C. Zhang, *Graded functionality obtained in NiTi shape memory alloy via a repetitive laser processing strategy.* J. Mat. Proc. Tech., **296**, 117177, (2021). https://doi.org/10.1016/j.jmatprotec.2021.117177
10. L. Motibane, L. Tshabalala, D. Hagedorn-Hansen, S. Chikosha, and T. Becker. Functional and Mechanical Behavior of Ultra-Thin, Porous NiTi Fabricated via Laser Powder Bed Fusion. In TMS Annual Meeting & Exhibition. Cham: Springer Nature Switzerland, TMS Annual Meeting, Orlando, Florida, USA, March 3-7 (2024), 96
11. Z. Yang, H. Wang, Y. Huang, X. Ye, J. Li, C. Zhang, H. Li, B. Pang, Y. Tian, C. Huang, G. Sun, Strain rate dependent mechanical response for monoclinic NiTi shape memory alloy: Micromechanical decomposition and model validation via neutron diffraction, Mater. & Design, **191**, 108656, (2020). https://doi.org/10.1016/j.matdes.2020.108656
12. J.C. Liu, H. Mei, F. Chen, L. Li, Y.X. Tong, Effect of Ta content on microstructure, martensitic transformation, and shape memory effect of (Ni52.2Ti47.8)100-xTax

alloys, Journal of Alloys and Compounds,**1003**, 175621, (2024).
https://doi.org/10.1016/j.jallcom.2024.175621